Received: 3 April 2018 | Revised: 15 May 2018 | Accepted: 12 June 2018

DOI: 10.1002/aoc.4503

FULL PAPER

WILEY Applied Organometallic Chemistry

Synthesis and cytotoxic evaluation of some substituted pyrazole zirconium (IV) complexes and their biological assay

Walaa H. El-Shwiniy | Wesam S. Shehab | Soha F. Mohamed | Hend G. Ibrahium

Department of Chemistry, Faculty of Science, Zagazig University, Zagazig 44519, Egypt

Correspondence
Walaa H. El-Shwiniy, Department of Chemistry, Faculty of Science, Zagazig University, Zagazig, 44519, Egypt.
Email: walaa1986@zu.edu.eg; wh595949@gmail.com

Pyrazole and their derivatives are found to have intense biological efficiency. In the present work some substituted pyrazole derivatives were synthesized and used as ligands (4-[2-vinylthiophene]-3-methyl pyrozolin-5(4H) - one (L_1), 4-[4-chloro benzylidine]-3-methyl pyrozolin-5(4H) - one (L_2) and 4-[4-dimethylnitro benzylidine]-3-methylpyrozolin-5(4H) - one (L_3)) to prepare the zirconium (IV) complexes. The synthesized ligands and their complexes were obtained as colored powdered materials and were characterized using magnetic measurements, melting point, molar conductance, infrared, electronic, ^{1}HNMR, mass spectra and thermogravimetric analyses. All of the tested compounds showed good microbial activity against pathogenic microorganisms. The tested compounds exhibited considerable antitumor activity and cytotoxic specificity towards human colon carcinoma cell line (HCT-116).

KEYWORDS
antitumor, complexes, pyrazole derivatives, spectral study, zirconium (IV)

1 | INTRODUCTION

Pyrazolone played a particular role due to both their broad spectrum of bioactivity and their wide ranging utility as synthetic tools in the design of various bioactive molecules. In recent years, substituted pyrazole derivatives have drawn considerable attention owing to their broad spectrum biological properties. Compounds with pyrazole functional units exhibit antimicrobial,[1] herbicidal,[2] antitumor,[3–5] insecticidal,[6–8] fungicidal[9] and antiviral activities.[10,11]Lamberth[12] has summarized the significance of pyrazole derivatives in crop protection chemistry, including herbicidally-, fungicidally- and insecticidally-active pyrazole classes. Moreover, some substituted pyrazole derivatives (L_1, L_2, L_3) had been synthesized, and the compound belongs to a very important class with pharmacological activity (Scheme 1).

The stability of the zirconium acyl complexes has been found to depend upon the nature of the co-ligands and decreases as the N-donor capacity of the co-ligand increases.[13] It is possible, therefore, that the use of stronger electron-donor ligands in place of C_5H_5 might facilitate displacement of an acyl ligand. Due to its wide range of biological activity, pyrazoles have received a considerable interest in the field of drug discovery and therefore pyrazole ring constitutes a relevant synthetic target in pharmaceutical industry. In fact, such a heterocyclic moiety represents the core structure of a number of drugs.

Therefore, in the present study, we investigated the coordination behavior of L_1, L_2, L_3 for Zr (IV) and the data are correlated with their thermal properties. In this vein, we have been developed novel pyrazole derivatives (L_1, L_2, L_3) and Zr (IV) in order to hopefully produce new compounds with antitumor activity. The as-prepared new compounds were designed, synthesized and characterized.

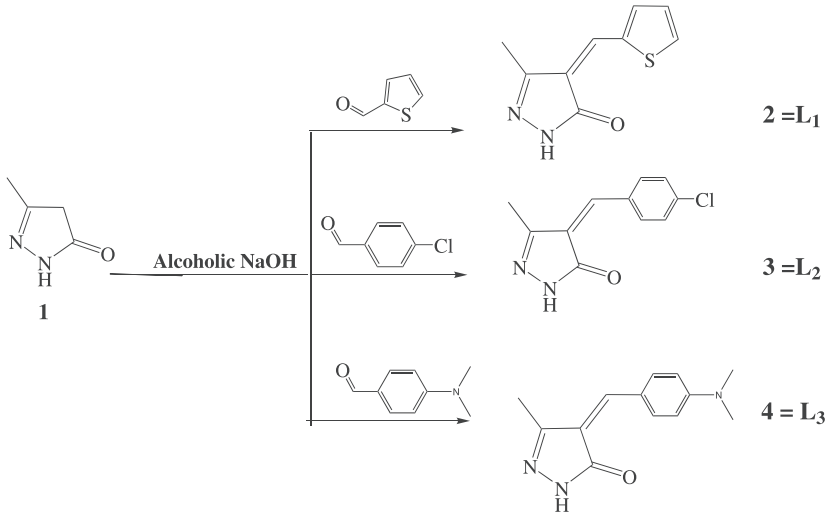

SCHEME 1 Structure of the synthesized compounds

2 | EXPERIMENTAL

2.1 | Materials and methods

2.1.1 | Chemicals

All chemicals used for the preparation of the complexes were of analytical reagent grade, commercially available from different sources and used without further purification. CHN analysis was executed on a Perkin Elmer CHN 2400. The percentages of the metal ions were determined gravimetrically by transforming the solid products into metal ion. The percentages of the metal ions were also estimated using an atomic absorption spectrometer. The spectrometer model was PYE-UNICAM SP 1900 and fitted with the corresponding lamp. IR spectra were recorded on FT-IR 460 PLUS (KBr discs) in the range from 4000–400 cm^{-1}. ^{1}H and ^{13}C NMR spectra were recorded on a Bruker 300 MHz NMR Spectrometer using tetramethylsilane (TMS) as the internal standard, chemical shifts are expressed in δ (ppm) and DMSO-d_6 was used as the solvent. TGA-DTG measurements were carried out with heating rate of 20°C min^{-1} under N_2 atmosphere from room temperature to 1000 °C using TGA-50H Shimadzu. The mass of sample was accurately weighted out in an aluminum crucible. Absorbance measurements were conducted on a double beam spectrophotometer (T80 U*V*/Vis) with wavelength range 190 nm ~ 1100 nm, spectral bandwidth of 2 nm. Magnetic measurements were carried out on a Sherwood scientific magnetic balance using Gouy balance using Hg [Co $(SCN)_4$] as calibrate. All melting points are uncorrected and were determined on a Gallen Kamp electric melting point apparatus. Molar conductivities of the solutions of the ligand and metal complexes in DMSO with concentrations of 1×10^{-3} M were measured on CONSORT K410. The completion of the reactions was confirmed using thin layer chromatography (TLC) on silica gel coated aluminum sheets.

2.2 | Synthesis

A series of 4-arylidene-3-methyl-5-pyrazolone derivatives have been synthesized by condensing 3-methyl-5-pyrazolone with substituted aromatic aldehydes as illustrated in Scheme 1. Structures of the synthesized compounds (**2–4**) as follow:

2.2.1 | Synthesis of 3-methyl-5-pyrazolone (Scheme 1)[14]

In this work take ethyl acetoacetate in a beaker and stirred magnetically and add to a solution of hydrazine hydrate in absolute alcohol.[14] The reaction mixture was kept at 60°C and the crystalline was separated after stirring for 1 hr at 60°C. The crystallization complete when the reaction mixture cooled in ice bath. Then crystalline solid was washed with cold alcohol and dried. The 3- methyl-5-pyrazolone so obtained was kept for next step of the synthetic scheme.[15] Yellow solid, Yield 81%, m.p.: 207–210°C. IR (KBr, *ν*, cm^{-1}): 2566.47 cm^{-1} (CH_3 group), 3283.05 cm^{-1} (N-H Stretch), 1609.91 cm^{-1} (CH=CHstretch), 1735.77 cm^{-1}, 1676.28 cm^{-1} (ketone group), 1342–1266 cm^{-1} (C-N stretch), 3000–2840 cm^{-1} (C-H stretch). ^{1}HNMR (DMSO-d_6, 300 MHz): δ = 0.265 (s, 1H, NH, Pyrazolonenucleus), δ, ppm: 1.652 (s, 2H, CH_2), δ, ppm: 0.8263 (s, 3H, CH_3). Anal. Calcd for $C_4H_6N_2O$ (98.1): C, 48.97; H, 6.16; N, 28.56; Found C, 48.96; H, 6.15; N, 28.56%.

2.2.2 | Synthesis of 3-methyl-5-pyrazolone derivatives[16–18]

Take synthesized pyrazolone in freshly prepared 20% sodium hydroxide (alcoholic solution) was poured into it and stirred magnetically for 30 min. Substituted aromatic aldehyde was added to the reaction mixture and kept under constant stirring for 8 hrs. Reaction

mixture was transferred to crushed ice and neutralizedwith dil. HCl to precipitate the product in Scheme 1. Synthesis of 3-methyl-5-pyrazolone (intermediate) via Knorrpyrazolone reaction and further reaction with substituted arylaldehydes to obtain 3-methyl-5-pyrazolone derivatives.[19]

2.2.3 | 4-[2-vinylthiophene]-3-methyl pyrozolin-5(4H) - one (L_1)

Black, m.p.: 260°C, Yield 79% IR (KBr, ν, cm^{-1}): 3413 (NH), 1595 (C=O), 1406 cm^{-1} (C=N) and 1011 cm^{-1} (C=S). ^{1}HNMR (DMSO-d_6, 300 MHz): δ = 1.98 (s, 3H, CH_3), 6.75 (S, 1H, =CH-Ar), 8.11 (d, 3H, Ar-H), 11.15 (s, 1H, -NH). Anal. Calcd for $C_9H_8N_2OS$ (192): C, 56.25; H, 4.16; N 14.58; S, 16.66; Found C, 56.00; H, 4.75; N, 14.55; S, 16.56%.

2.2.4 | 4-[4-chloro benzylidine]-3-methyl pyrozolin-5(4H) - one (L_2)

Yellow, m.p.: 240°C, Yield 84% IR (KBr, ν, cm^{-1}): 3413 (NH), 1590 (C=O) and 1406 cm^{-1} (C=N). ^{1}H NMR (DMSO-d_6, 300 MHz): δ = 1.88 (s, 3H, CH_3), 6.51 (S, 1H, =CH-Ar), 7.39 (m, 4H, Ar-H), 8.64 (s, 1H, -NH). Anal. Calcd for $C_{11}H_9N_2OCl$ (220.5): C, 59.86; H, 4.08; N 12.69; Cl, 16.09; Found C, 59.42; H, 4.03; N, 12.26; Cl, 16.00%.

2.2.5 | 4-[4-dimethylnitro benzylidine]-3-methylpyrozolin-5(4H)- one (L_3)

Orange, m.p.: 180°C, Yield 65% IR (KBr, ν, cm^{-1}): 3418 (NH), 1613 (C=O) and 1406 cm^{-1} (C=N). ^{1}H NMR (DMSO-d_6, 300 MHz): δ = 1.91 (s, 3H, CH_3), 3.71 (s, 6H, -N $(CH_3)_2$), 6.51 (S, 1H, =CH-Ar), 7.51–7.60 (m, 4H, Ar-H), 8.97 (s, 1H, -NH). Anal. Calcd for $C_{13}H_{15}N_3O$ (229.14): C, 68.08; H, 6.54; N 18.32; Found C, 68.07; H, 6.13; N, 18.10.

2.2.6 | $[ZrO(L_1)Cl]Cl\cdot H_2O$

Grey; Yield: 77%; m.p.: 120°C; M.Wt: 580.22; Elemental analysis for $ZrC_{18}H_{18}N_4O_4S_2Cl_2$: found, C, 38.16; H, 3.02; N, 9.37; Zr, 16.00; Cl, 12.83. Calcd, C, 38.41; H, 3.10; N, 9.69; Zr, 16.22; Cl, 12.62; Λ_m = 99.50 S cm^2 mol^{-1}; IR (KBr, ν, cm^{-1}): 3390 m,br (NH), 1600 m (C=O), 1457vw cm^{-1} (C=N) and 1054 m cm^{-1}(C=S), 544w and 492w (M–N). ^{1}HNMR (DMSO-d_6, 300 MHz): δ = 2.49 (s, 3H, CH_3), 3.42 (s, 2H, H_2O), 6.75 (S, 1H, =CH-Ar), 8.11 (d, 3H, Ar-H).

2.2.7 | $[ZrO(L_2)Cl]Cl\cdot H_2O$

Orange; Yield: 81%; m.p.: 296°C; M.Wt: 637.22; Elemental analysis for $ZrC_{22}H_{20}N_4O_4Cl_4$: found, C, 42.33; H, 3.12; N, 9.00; Zr, 14.21; Cl, 22.43. Calcd, C, 42.63; H, 3.31; N, 9.04; Zr, 14.73; Cl, 22.93; Λ_m = 89.00 S cm^2 mol^{-1}; IR (KBr, ν, cm^{-1}): 3400 m,br (NH), 1599 m (C=O), 1421 m cm^{-1} (C=N) and 638w and 539w (M–N). ^{1}HNMR (DMSO-d_6, 300 MHz): δ = 2.07 (s, 3H, CH_3), 7.33 (S, 1H, =CH-Ar), 7.37–7.94 (d, 3H, Ar-H), 3.46 (s, 2H, H_2O).

2.2.8 | $[ZrO(L_3)Cl]Cl\cdot H_2O$

Brown; Yield: 69%; m.p.: 110°C; M.Wt: 654.50; Elemental analysis for $ZrC_{26}H_{32}N_6O_4Cl_2$: found, C, 48.99; H, 4.41; N, 9.00; Zr, 14.15; Cl, 11.05. Calcd, C, 49.01; H, 4.88; N, 13.19; Zr, 14.33; Cl, 11.15; Λ_m = 91.51 S cm^2 mol^{-1}; IR

TABLE 1 Some selected Infrared frequencies[a] (cm^{-1}) and tentative assignments[b] for L_1, L_2, L_3 and their complexes.

L_1	$[ZrO(L_1)_2Cl]Cl\cdot H_2O$	L_2	$[ZrO(L_2)_2Cl]Cl\cdot H_2O$	L_3	$[ZrO(L_3)_2Cl]Cl\cdot H_2O$	Assignments[b]
-	$3397_{v,br}$	-	$3402_{m,br}$	-	$3399_{m,br}$	ν(O-H); H_2O
$3413_{m,br}$	$3390_{m,br}$	$3413_{m,br}$	$3400_{m,br}$	$3413_{m,br}$	$3399_{m,br}$	ν(N-H); -NH
3093_w	3090	3070_m	3070	3060_w	3065	ν(C-H); aromatic
2917_m	2917	2925_m	2925	2917_m	2915	ν(C-H); aliphatic
1595_{ms}	1600_m	$1590_{m,sh}$	1599_m	1613_{vs}	1615_m	ν(C=O)
1406_m	1457_s	1406_s	1421_m	1406_m	1433_{vw}	ν(C=N),
1406_m	1430_s	1491_m	1450_m	1400_m	1410_{vw}	ν(C=C)
-	830 m	-	833w	-	862 m	ν(Zr = O)
-	544	-	638	-	593	ν(M-N)
-	492	-	539	-	543	
-	-	-	680 s	-		

[a]s = strong, w = weak, v = very, m = medium, br = broad, sh = shoulder,

[b]ν = stretching, δ_b = bendin, δ_r = rocking.

(KBr, ν, cm^{-1}): 3399 m,br (NH), 1615 m (C=O) and 1433vw cm^{-1} (C=N) and 593w and 543w (M–N). ^{1}HNMR (DMSO-d_6, 300 MHz): δ = 1.84 (s, 3H, CH_3), 2.11–2.54 (s, 6H, -N $(CH_3)_2$), 7.64 (S, 1H, =CH-Ar), 7.45–7.64 (m, 4H, Ar-H), 3.40 (s, 2H, H_2O).

2.3 | Biological activity and in vitro cytotoxicity assays

The procedures of antibacterial activity assay were evaluated according to the literature.[20] The synthesized compounds were tested against colon carcinoma cell line (HCT-116).[21] Antitumor viability assay was performed by the described method by Saintigny and Monnat Jr.[22]

3 | RESULTS AND DISCUSSION

The complexes of L_1, L_2, L_3 with Zr(IV) were prepared and studied. Depending on elemental analysis, the molar ratio of the prepared complexes was determined. Conductance measurements, magnetic susceptibilities and spectral measurements were different parameters used to obtain the geometry and formulas of prepared complexes. From magnetic measurments, the prepared complexes have diamagnetic properties. For Zr(IV) complexes and its corresponding ligands, the conductivity measurements were done in DMSO at 1.0 × 10P^{-3}PM and were found from 5.03 to 99.50 S cm^2 mol^{-1}[23] and it indicated that they were electrolytes.[24–26] Chloride ion was found as counter ions for the isolated complexes and this was agreed with IR-data and molar conductance.

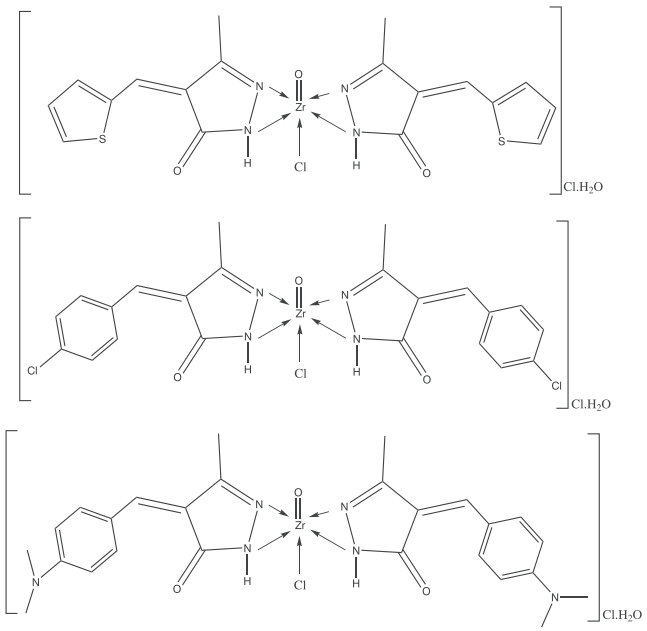

SCHEME 2 The proposed structures of the synthesized complexes

3.1 | Infra-red Spectra analysis

The infra-red spectra for the three free ligands (L_1, L_2, L_3) and their metal complexes were showed in Figure S1 and listed in Table 1. From these spectra the site and kind of

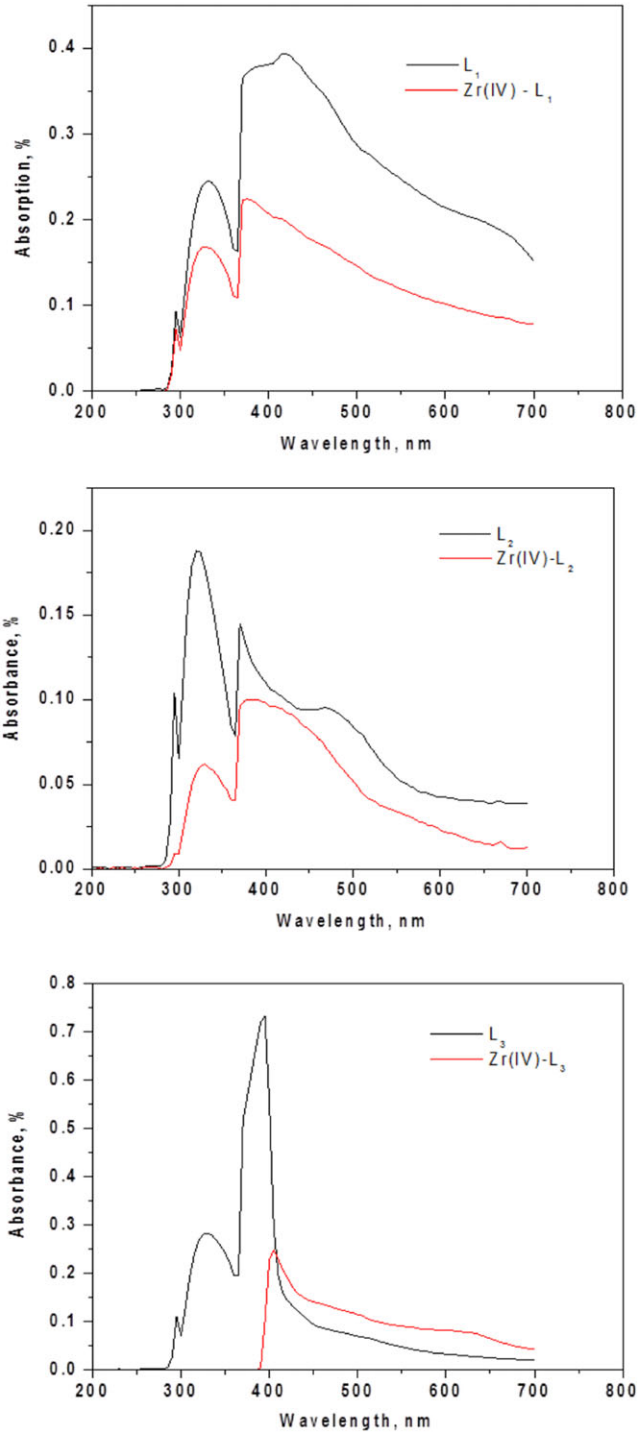

FIGURE 1 Electronic absorption for L_1, [ZrO $(L_1)_2$Cl]Cl•H_2O, L_2, [ZrO $(L_2)_2$Cl]Cl•H_2O, L_3 and [ZrO $(L_3)_2$Cl]Cl•H_2O

donation that may be involved in chelation could be identified.[27,28] At 3413 and 1406 cm^{-1} two bands attributed to the stretching vibration of ν(N-H) amino and for ν(C=N) hydrazono groups. i.e. respectively for L_1, L_2, L_3.[29,30] From shifting to higher and lower frequency values for ν(C=N), the coordination between the ligand molecule and Zr(IV) through the nitrogen atom of hydrazono group was confirmed. The following higher frequencies (1457, 1421 and 1433) values of ν(C=N) may indicate an increase of C=N bond strength as a result of coordination.

Upon coordination to Zr(IV) the electron density on the nitrogen atom was decreased this lead to a decrease in the electron repulsion between the nitrogen lone pair and the double bond electrons and as a result C=N bond became a strong band with a higher frequency.[29–31] A lower frequency value (3390, 3400 and 3399 cm^{-1}) for the shifting of ν(N-H) indicated a decrease of the N-H bond strength upon coordination.[29] These changes of the IR spectra suggest that L_1, L_2, L_3 are coordinated to the Zr(IV) via two nitrogen atoms of amino (N-H) and hydrazono (C=N) groups. The ν(O-H) vibration of the water molecules in the prepared complexes were found at 3397–3402 cm^{-1}[27–33] also, the ν(C=O) was found at 1599–1615 cm^{-1}.

A group of new bands with different intensities was found which characteristics for ν(M-N). The ν(M-N) bands observed at 544, 492 cm^{-1} for Zr(IV)-L_1, 638, 539 cm^{-1} for Zr (IV)-L_2 and 593 and 543 cm^{-1} for Zr(IV)-L_3, which are absent in the spectra of L_1, L_2 and L_3.[27–34] From the above mentioned result the coordination of L_1, L_2, and L3 was done through two C=N and N-H groups (Scheme 2).

3.2 | UV–Vis. spectra

From the UV–Visible data of the ligands (L_1, L_2, and L_3) and their Zr(IV) chelates in the wavelength interval from 200 to 800 nm were recorded (Table S1 and Figure 1). The spectra of the three ligands was absorbed by three absorption bands at 245, 283 and 282 nm. Which attributed to π-π^*(phenyl ring) transition also, the three bands at 330 nm are assigned to n-π^* (-C=O,-NH and –C=N) transition, in case of unsaturated hydrocarbons obtained by cyanide and ketone group,[26] occur slightly shifted to lower values (hypsochromic shift) and wavelength (bathochromic shift), when ligands and metal cheated new bands appear in reflection spectra of complexes refer to the metal complexes were formed these new bands shown in the range from 375 to 487 nm which may be assigned to the ligand to metal charge-transfer.[35,36]

3.3 | Nuclear magnetic resonance (^{1}HNMR)

The ^{1}H NMR spectra of L_1 and their metal complex (Figure S2 (A, B)) confirm the suggested structures. The proton of –NH signal for ligand observed at δ: 11.15 ppm (s, 1H, –N<u>H</u>, exchange with D_2O) showed no observed it in complex. This enhances the hypothesis that –NH is the coordinating group. The new signal are observed in δ: 3.42 ppm due to presence of H_2O molecule in complex. On the other hand, the values of protons of -CH aliphatic (methyl) observed in δ: 1.978 ppm (s, 3H, –C<u>H</u>$_3$), that of aromatic ring are in δ: 8.11 ppm (d, 3H, Aromatic–<u>H</u>) and the proton of (=CH-Ar) group observed in δ: 6.75 ppm (S, 1H, =CH-Ar) increased and the intensity of signals is increased, as shown in Table 2.[37] From ^{1}HNMR and FT-IR results, it was proposed that the L_1 coordinated to the central metal ion as bidentate ligand through the two nitrogen atom of pyrazolone group.[35]

The ^{1}HNMR spectra of L_2 and their metal complex (Figure S2 (C, D)) confirm the suggested structures. The proton of –NH signal for ligand observed at δ: 8.64 ppm (s, 1H, –N<u>H</u>, exchange with D_2O) showed no observed it in complex. This enhances the hypothesis that –NH is the coordinating group. The new signalare observed in δ: 3.46 ppm due to presence of H_2O molecule in complexes. On the other hand, the values of protons of -CH aliphatic (methyl) observed in δ: 1.88 ppm (s, 3H, –C<u>H</u>$_3$), that of aromatic ring are in δ: 7.39 ppm (m, 4H, Aromatic–<u>H</u>) and the proton of (=CH-Ar) group observed in δ: 6.51 ppm (S, 1H, =CH-Ar) increased and the intensity of signals is increased, as shown in

TABLE 2 Selected ^{1}HNMR data of L_1, L_2, L_3 and their diamagnetic complexes

Compounds	δ H; H_2O	δH; -CH aliphatic (methyl)	δH; -CH aromatic	δH; =CH aromatic	δH;-N $(CH_3)_2$	δH; -NH hydrazid
L_1	-	1.978	8.105	6.75	--	11.159
L_1/Zr(IV)	3.418	2.49	8.155	6.641	--	--
L_2	-	1.88	7.37–7.39	6.513	--	8.64
L_2/Zr(IV)	3.469	2.074	7.307	7.33	--	--
L_3	-	1.91	7.51–7.603	6.505	3.718	8.97
L_3/Zr(IV)	3.400	1.84	7.453	7.640	2.11–2.54	--

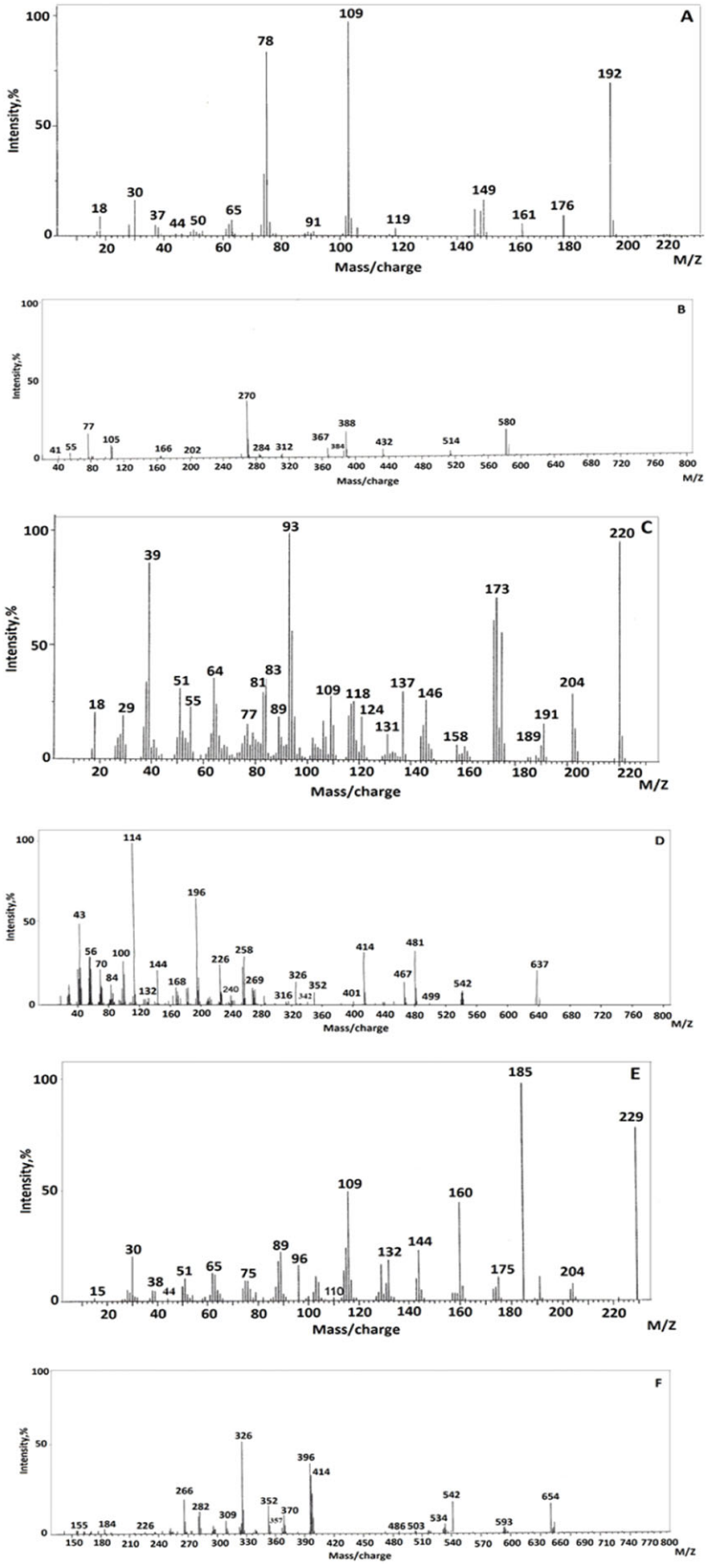

FIGURE 2 Mass spectra diagrams for (A) L_1, (B) $[ZrO(L_1)_2Cl]Cl{\bullet}H_2O$, (C) L_2, (D) $[ZrO(L_2)_2Cl]Cl{\bullet}H_2O$, (E) L_3 and (F) $[ZrO(L_3)_2Cl]Cl{\bullet}H_2O$

Table 2. From ^{1}HNMR and FT-IR results, it was proposed that the L_2 coordinated to the central metal ion as bidentate ligand through the two nitrogen atom of pyrazolone group.[28]

The ^{1}HNMR spectra of L_3 and their metal complex (Figure S2 (E, F)) confirm the suggested structures. The proton of –NH signal for ligand observed at δ: 8.97 ppm (s, 1H, –NH, exchange with D_2O) showed no observed it in complex. This enhances the hypothesis that –NH is the coordinating group. The new signal are observed in δ: 3.40 ppm due to presence of H_2O molecule in complex. On the other hand, the values of protons of -CH aliphatic (methyl) observed in δ: 1.91 ppm (s, 3H, –CH_3), that of aromatic ring are in δ: 7.51–7.60 ppm (m, 4H, Aromatic–H),the proton of (=CH-Ar) group observed in δ: 6.51 ppm (S, 1H, =CH-Ar) and protons of (N $(CH_3)_2$) group observed in δ: 3.71 ppm (s, 6H, -N $(CH_3)_2$) increased and the intensity of signals is increased, as shown in Table 2. From ^{1}HNMR and FT-IR results, it was proposed that the L_3 coordinated to the central metal ion as bidentate ligand through the two nitrogen atom of pyrazolone.[30]

3.4 | Thermal studies

The most commonly used thermal analysis techniques are thermogravimetry (TG) for the characterization of both organic and inorganic materials. TG measurements give fundamental information about the thermal properties of the chelates. Representative thermogravimetric curves are shown in Figure 2. The maximum temperature values, T_{max}/°C, together with the corresponding weight loss for each step of decomposition of the compounds together with theoretical percentage mass losses are given in Table 3 (Figure 3).

The thermal decomposition for the ligand (L_1) started at 44°C and finished at 601°C with two stages. The first stage of degradation takes place at maximum temperature of 133, 276 and 532°C is accompanied by a total weight loss of 83.134%, close to the calculated value 83.33%. Corresponding to loss of $4C_2H_2 + CO + N_2$ molecule and activation energy of 105.29 KJ mol^{-1} (endothermic). The second step of decomposition occurs at maximum 544°C and the actual weight loss from these step is 16.866%, close to the calculated value 16.66% corresponding to value of S.

The thermal degradation of $[ZrO(L_1)_2Cl]Cl•H_2O$ complex occurs in two degradation stages, the first stage of decomposition occurs at maximum 94°C and is accompained by a weight loss of 3.10% corresponding to loss of H_2O with an activation energy 47.06 KJ mol^{-1}. The second step of decomposition occurs at different temperatures and is accompanied by a weight loss of 81.17%; corresponding to thevalue of $8C_2H_2 + 2CO + 2\ N_2 + Cl_2 + S_2O$ theoretically, the weight loss in this step 81.69%. The experimental value of 15.72% corresponding to Zr agrees with the calculated value 15.22%.

The thermal degradation for the ligand (L_2) started at 43°C and finished at 642°C with one stage. This stage is accompanied by total weight loss of 90.185%, close to the calculated value 89.115%. Corresponding to loss of $4C_2H_2 + HCl + CO + N_2$ molecule and

TABLE 3 Thermogravimetric data of L_1, L_2, L_3 and their metal complexes

			% Estimated (calculated)		Assignment
Compounds	**Decomposition**	**DTG $_{max}$ (°C)**	**Mass loss**	**Total mass loss**	**Lost species**
L_1	First step	133,276,532,544	83.134 (83.33)	83.134 (83.33)	$4C_2H_2 + CO + N_2$
192, $C_9H_8ON_2S$	Residue		16.866 (16.66)		S
$[ZrO(L_1)_2Cl]Cl•H_2O$	First step	94	3.10 (3.08)	84.27 (84.77)	H_2O
580.22, $ZrC_{18}H_{18}N_4O_4S_2Cl_2$	Second step	281,422,744,809	81.17 (81.69)		$8C_2H_2 + 2CO + 2\ N_2 + Cl_2 + S_2O$
	Residue		15.72 (15.22)		Zr
L_2	First step	237,642	90.185 (89.115)	90.185 (89.115)	$4C_2H_2 + HCl + CO + N_2$
220.5, $C_{11}H_9N_2OCl$	Residue		9.815 (10.88)		2C
$[ZrO(L_2)_2Cl]Cl•H_2O$	First step	78	2.82 (2.78)	83.79 (83.08)	H_2O
637.22, $ZrC_{22}H_{20}O_4N_4Cl_4$	Second step	286,557,660	80.97 (80.30)		$9C_2H_2 + 2\ N_2 + 3CO + 2Cl_2$
	Residue		16.198 (16.66)		Zr + C
L_3	First step	323,568,901	100 (99.82)	100 (99.82)	$6C_2H_2 + CO + NH_3 + N_2$
229.14, $C_{13}H_{15}ON_3$					
$[ZrO(L_3)_2Cl]Cl•H_2O$	First step	80	2.75 (2.60)	86.06 (85.76)	H_2O
654.5, $ZrC_{26}H_{32}O_4N_6Cl_2$	Second step	192,299,563,551,873	83.31 (83.16)		$11C_2H_2 + 2C_2H_4 + Cl_2 + 3N_2O$
	Residue		13.93 (13.33)		Zr

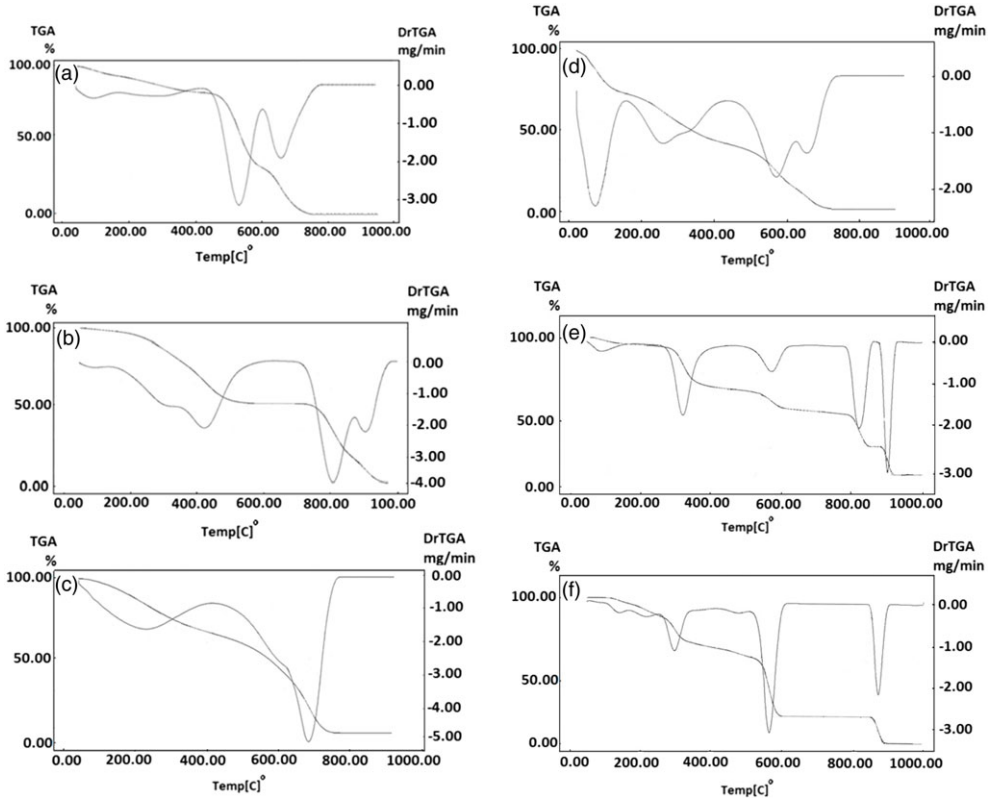

FIGURE 3 TGA and DTG diagrams for (a) L_1, (b) $[ZrO(L_1)_2Cl]Cl{\bullet}H_2O$, (c) L_2, (d) $[ZrO(L_2)_2Cl]Cl{\bullet}H_2O$, (e) L_3 and (f) $[ZrO(L_3)_2Cl]Cl{\bullet}H_2O$

activation energy of 14.07 KJ mol^{-1} (endothermic). The Residue value decomposition occurs at maximum 642°C and the actual weight loss from these step is 9.815%, close to the calculated value 10.88% corresponding to 2C.

The thermal degradation of $[ZrO(L_2)_2Cl]Cl{\bullet}H_2O$ complex takes place in two degradation stages, the first stage of decomposition occurs at maximum 78°C and is accompained by a weight loss of 2.82% corresponding to loss of H_2O with an activation energy 25.91 KJ mol^{-1}. The second step of decomposition occurs at different temperatures is 286, 557, 660°C and is accompanied by a weight loss of 80.97%; corresponding to the value of $9C_2H_2 + 3CO + 2\ N_2 + Cl_2$ theoretically, the weight loss in this step 80.30%. The experimental value of 16.198% corresponding to Zr + 2C agrees with the calculated value 16.66%.

The thermal decomposition for the ligand (L_3) started at 47°C and finished at 901°C with one stage. This stage is accompanied by a total weight loss of 100%, close to the calculated value 99.82% corresponding to loss of $6C_2H_2 + NH_3 + CO + N_2$ molecule and an activation energy of 75.13 KJ mol^{-1} (endothermic).

The thermal degradation of $[ZrO\ (L_3)_2Cl]Cl{\bullet}H_2O$ complex occurs in two degradation stages, the first stage of decomposition occurs at maximum 80°C and is accompained by a weight loss of 2.75% corresponding to loss of H_2O with an activation energy 46.32KJ mol^{-1}. The second step of decomposition happens at different temperatures is 192, 299, 551, 563, 873°C and is accompanied by a weight loss of 83.31%; corresponding to the value of $11C_2H_2 + 2C_2H_4 + 3N_2O + Cl_2$ theoretically, the weight loss in this step 83.16%. The experimental value of 13.93% corresponding to Zr agrees with the calculated value 13.33%.

3.5 | Kinetic data

Activation energies, E*, entropies, ΔS*, enthalpies, ΔH*, and Gibbs free energies, ΔG* below to kinetic thermodynamic parameters. The Coats-Redfern (CR) and Horowitz-Metzger (HM) relationships used to estimate graphically by employing for the decomposition.[37,38] Their parameters were detected using the above mentioned methods by graphical means and they are listed in Table 4. The activation energies of decomposition were found to be in the range 35.33–137.93 kJ mol^{-1}. The maximum values of the activation energies refer to the thermal stability of the complexes, while the negative values of entropy of activation indicate that all complexes with decomposition reactions proceeded with a lower rate than the normal ones (Figure 4). From the kinetic data obtained DTG curves, all the chelates had negative entropy, which refer that activated complexes have more ordered systems than reactants.

TABLE 4 Thermal behavior and kinetic parameters determined using the Coats–Redfern (CR) and Horowitz–Metzger (HM) operated for L_1, L_2, L_3 and their complexes

Compounds	Decomposition Range (K)	T_s (K)	Method	Parameter E^* (KJ/mol)	A (s^{-1})	ΔS^* (KJ/mol. K)	ΔH^* (KJ/mol)	ΔG^* (KJ/mol)	R[a]	SD[b]
L_1	672–873	805	CR	105.296	368.535×10^3	−446.853	98.597	458.319	0.885	0.433
($C_9H_8N_2OS$)			HM	137.726	107.982×10^3	−436.647	131.033	482.533	0.933	0.177
	876–1029	939	CR	249.270	7.022×10^6	−469.744	241.463	682.865	0.938	0.283
			HM	268.430	1.531×10^6	−457.413	260.623	690.133	0.923	0.170
$[ZrO(L_1)_2Cl]Cl \cdot H_2O$	473–603	554	CR	47.065	21.787×10^3	−426.446	42.459	278.710	0.912	0.266
($ZrC_{18}H_{10}N_4O_4S_2Cl_2$)			HM	59.294	44.212×10^3	−432.329	54.688	294.198	0.906	0.139
	625–807	695	CR	95.414	6.276×10^5	−452.502	89.635	404.124	0.968	0.185
			HM	99.884	3.904×10^6	−467.701	94.105	419.157	0.958	0.117
L_2	316–689	510	CR	14.076	8.267×10^3	−476.509	9.835	252.853	0.972	0.126
($C_{11}H_9N_2OCl$)			HM	24.303	8.633×10^3	−419.466	20.06	233.990	0.956	0.117
	709–997	915	CR	94.210	13.481×10^3	−418.283	86.600	469.331	0.944	0.308
			HM	117.980	45.024×10^4	−447.453	110.372	519.792	0.984	0.072
$[ZrO(L_2)_2Cl]Cl \cdot H_2O$	292–429	351	CR	25.910	4.968×10^3	−417.949	22.991	169.691	0.948	0.243
($ZrC_{22}H_{20}N_4O_4Cl_4$)			HM	30.666	5.354×10^3	−418.573	27.747	174.666	0.935	0.145
	720–898	830	CR	108.755	357.423×10^3	−446.344	101.854	472.319	0.980	0.165
			HM	127.947	323.088	−445.504	121.047	490.814	0.982	0.077
L_3	533–721	596	CR	75.131	157.916×10^3	−442.306	70.225	333.840	0.802	0.574
($C_{13}H_{15}N_3O$)			HM	74.134	385.385×10^3	−449.724	69.178	337.211	0.795	0.286
	779–981	841	CR	144.306	25.408×10^3	−424.253	137.310	494.110	0.921	0.329
			HM	144.632	115.609×10^3	−436.850	137.639	505.030	0.925	0.152
$[ZrO(L_3)_2Cl]Cl \cdot H_2O$	317–521	465	CR	46.320	73.252×10^3	−437.983	42.453	246.116	0.982	0.115
$ZrC_{26}H_{32}N_6O_4Cl_2$			HM	54.193	180.209×10^3	−445.467	50.326	257.469	0.990	0.0432
	537–687	572	CR	87.957	7.145×10^3	−416.911	83.201	321.674	0.802	0.496
			HM	87.266	14.597×10^3	−422.850	82.510	324.380	0.790	0.243

[a]= correlation coefficients of the Arrhenius plots and

[b]= standard deviation

3.6 | Mass spectra

Mass spectrometry was found benefit as a complementary method. Mass spectrum of the L_1 is in a good agreement with the suggested structure (Scheme 3), (Figure 2). The L_1 showed molecular ion peak ($M^{+\cdot}$) with m/z = 192 (71.00%) and M^{+1} at m/z = 193 (7.1%). The molecular ion peak [a] losses C_4H_3S to give fragment [b] at m/z = 109 (99.9%), molecular ion peak [b] lossesCH$_3$O to give fragment [c] at m/z = 78 (83.3%) and this [c] losses CH to give fragment [d] at m/z = 65 (7.2%). Also it loses [O] to give fragment [E] at m/z = 176 (9.1%). The molecular ion peak [a] losses CH_3O to give fragment [F] at m/z = 161 (6%).

The mass spectra of Zr(IV) complex displayed molecular peak at m/z = 580 (20.2%), suggesting that the molecular weight of the assigned product matching with elemental and thermogravimetric analyses (Scheme 4), (Figure 2).

Fragmentation pattern of the complex $[ZrO(L_1)_2Cl]Cl \cdot H_2O$ is given as an example in Scheme S1. The molecular ion peak [a] was appeared at m/z = 580 (20.2%) lossed $C_{10}H_8S_2$ to give [b] at m/z = 388 (16.43%). The molecular ion peak [a] losses $C_9H_9O_2S_2$ to give [C] at m/z = 367 (6.3%) and it losses [$C_{10}H_{12}S_2$] to give [d] at m/z = 384 (10%).

The mass spectrum of the L_2 displayed molecular structure is given as an example in (Scheme S2), (Figure 2). The molecular ion peak [a] appeared at m/z = 220 (96.1%), it lose C_6H_4Cl to give [b] at m/z = 109 (28%), Then a molecular ion peak [b] lossed $CH_3O$to give [c] at m/z = 78 (6.5%) and molecular ion peak [c] loss CH to give fragment [d] at m/z = 65 (24.3%) alsothe molecular ion peak [a] loses [O] to give [e] at m/z = 204 (4.5%) then [e] loss CH_3 to give [f] at m/z = 189 (1.6%) and it loss C_7H_5Cl to give fragment [g] at m/z = 96 (2.4%) then a molecular ion peak [g] loss CH_3 to give [h] at m/z = 81 (35.9%).

Fragmentation pattern of the complex $[ZrO(L_2)_2Cl]Cl \cdot H_2O$ is given as an example in (Scheme S3), (Figure 2). The molecular ion peak [a] appeared at m/z = 637 (21.5%) it loss $C_{12}H_8Cl_2$ to give fragment [b]

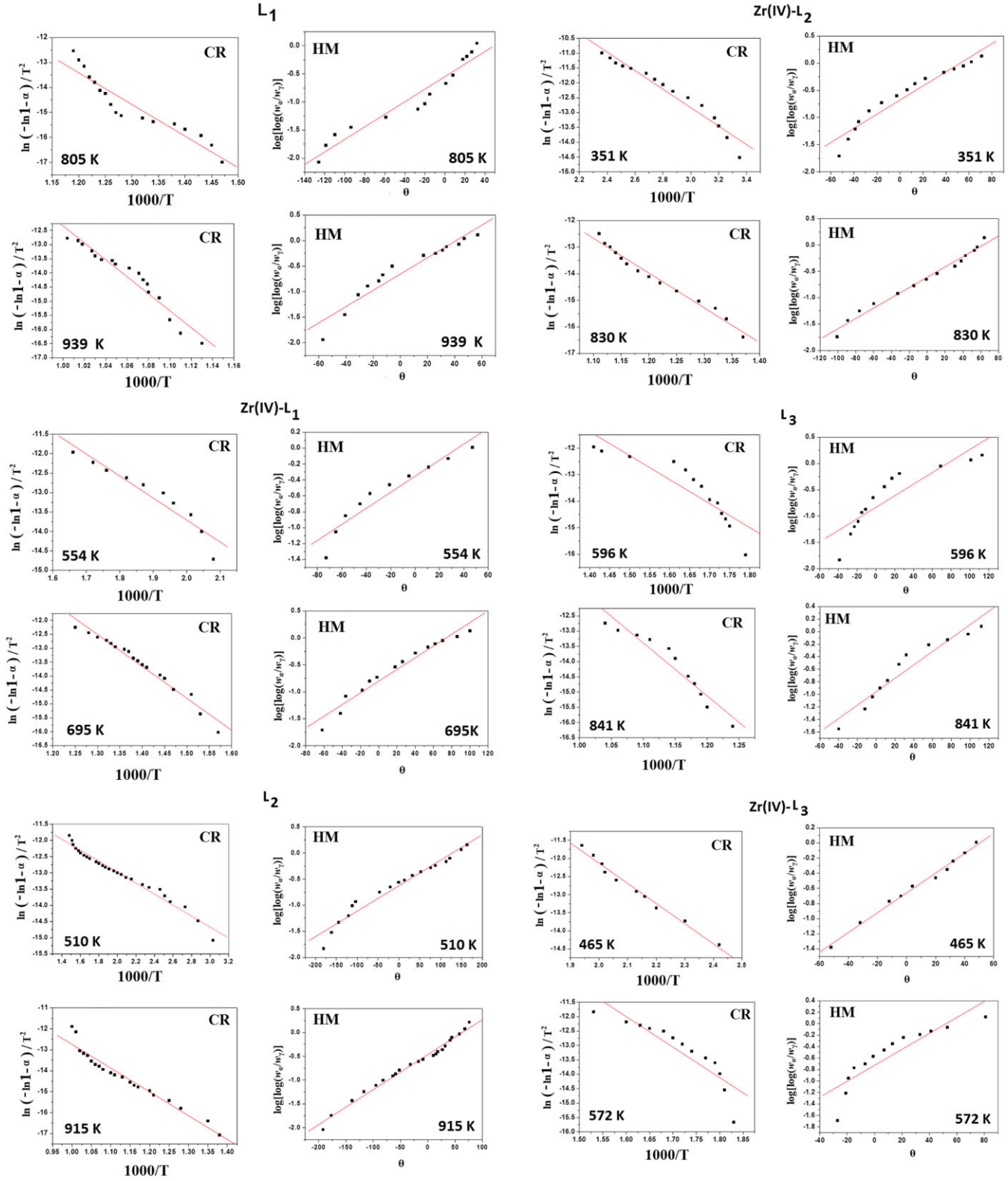

FIGURE 4 The diagrams of kinetic parameters of L_1, $[ZrO(L_1)_2Cl]Cl{\bullet}H_2O$, L_2, $[ZrO(L_2)_2Cl]Cl{\bullet}H_2O$, L_3 and $[ZrO(L_3)_2Cl]Cl{\bullet}H_2O$ using Coats-Redfern (CR) and Horowitz-Metzger (HM) equations

at m/z = 414 (31.2%), then molecular ion peak [b] loss $C_2H_6O_2$ to give [c] at m/z = 352 (14%) then [c] losses C_2H_2 to give [d] at m/z = 326 (18%).

The mass spectrum of the L_3 displayed molecular structure is given as an example in (Scheme S4), (Figure 2). The molecular ion peak [a] appeared at m/z = 229 (78.3%), it

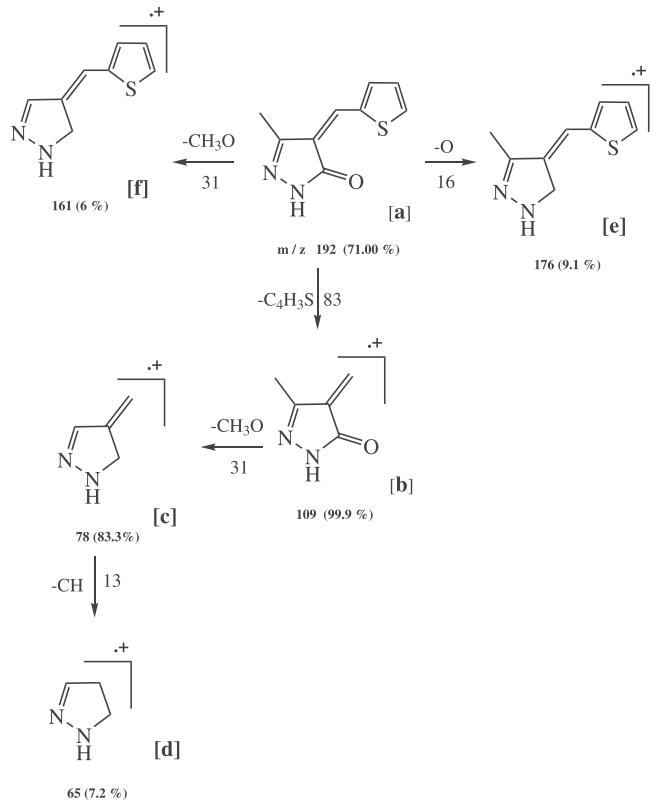

SCHEME 3 Fragmentation pattern of L_1

lose N $(CH_3)_2$ to give [b] at m/z = 185 (99%), Then a molecular ion peak [b] lossed C_6H_4 to give [c] at m/z = 109 (7%), molecular ion peak [c] loss CH_3O to give fragment [d] at m/z = 78 (5.5%) and ion [d] loss CH to give [e] at m/z = 65 (12.5%) also the molecular ion peak [a] loss $C_9H_{11}N$ to give [F] at m/z = 96 (25%) then [f] loss [O] to give [g] at m/z = 80 (1.4%) and molecular ion peak [g] loss CH_3 to give [h] at m/z = 65 (12.5%).

Fragmentation pattern of the complex $[ZrO(L_3)_2Cl]Cl{\bullet}H_2O$ is given as an example in (Scheme S1), (Figure 2). The molecular ion peak [a] appeared at m/z = 654 (20%) it loss $C_{16}H_{20}N_2$ to give fragment [b] at m/z = 414 (10.2%), then molecular ion peak [b] loss C_2H_4O to give [c] at m/z = 370 (5.2%) and molecular ion peak [c] loss C_2H_4O to give [d] at m/z = 326 (57.8%). Then a molecular ion peak [a] losses $C_{19}H_{25}N_2O$ to give [E] at m/z = 357 (9%).

3.7 | Antimicrobial efficiency

In this experiment, the antimicrobial potency of the free ligands (L_1, L_2, L_3) and their complexes, this studies were carried out on, *E. Coli* ATCC11229, *Coliform* ATCC8729, *S. aureus* ATCC6538, and *Salmonella typhi* ATCC14028 and antifungal screening was studied against two species, *Aspergillus niger* and *Pencillum expansum*, and detected by measuring size of the inhibitions zone (Table 5) according to the results of the antimicrobial study of the three ligands and their metal complexes have inhibitory action against all types of organism (Figure 5).

The Zr(IV) – $(L_1)_2$ complex showed a significant difference against *E. Coli* ATCC11229 than its free ligand.

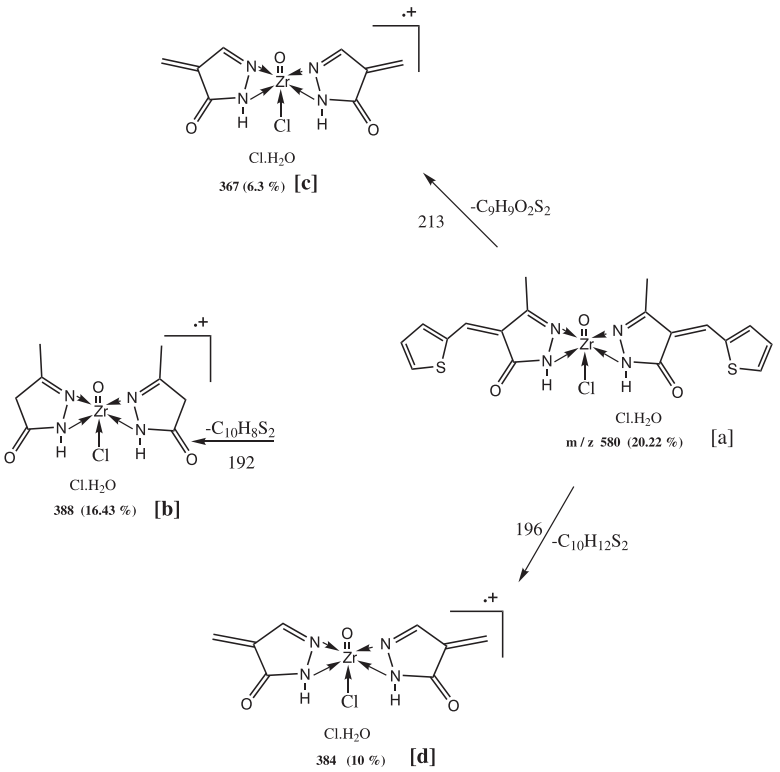

SCHEME 4 Fragmentation pattern of $[Zr(L_1)_2a]a{\bullet}H_2O$

TABLE 5 The inhibitation diameter zone values (mm) for L_1, L_2, L_3 and their complexes

Compounds		Microbial species					
		Bacteria				fungi	
		E. coli	Coliform	S. aureus	Salmonella typhi	A.niger	P.expansum
L_1		$9.3^{+1} \pm 0.67$	$9.3^{+1} \pm 0.88$	$29^{+3} \pm 2.2$	$9.3^{+1} \pm 0.91$	NA	$18^{+2} \pm 1.6$
L_1/Zr (IV)		$28^{+3} \pm 2.7$	$15.3^{+2} \pm 1.3$	NA	$21^{+3} \pm 2.4$	NA	NA
L_2		$15^{+1} \pm 1.2$	$7.4^{+1} \pm 0.8$	$21^{+2} \pm 2.5$	$9.3^{+1} \pm 1.1$	$11.3^{+1} \pm 0.85$	$15.3^{+1} \pm 0.78$
L_2/Zr (IV)		$22^{+2} \pm 25$	$14^{+2} \pm 1.3$	$26^{+3} \pm 2.2$	$15^{+2} \pm 1.1$	NA	NA
L_3		$14^{+1} \pm 1.3$	$9.3^{+1} \pm 0.56$	$15^{+1} \pm 1.1$	$12.6^{+1} \pm 1.5$	NA	NA
L_3/Zr (IV)		$22^{+2} \pm 2.1$	$12^{+1} \pm 1.1$	$30.3^{+3} \pm 2.6$	$20.6^{+3} \pm 2.6$	$20^{+3} \pm 1.9$	NA
$ZrOCl_2.8H_2O$		00	00	00	00	00	00
Control (DMF)		00	00	00	00	00	00
Standard	Nystain	00	00	00	00	11 ± 1.2	00
	Fluconazole	00	00	00	00	00	00
	Amoxycillin/Clavulanic	17 ± 1.2	14 ± 0.96	19 ± 1.1	00	00	00
	Cetaxime	00	00	00	00	00	00

Statistical significance P^{NS} – P not significant, $P > 0.05$; P^{+1} – P significant, $P < 0.05$; P^{+2} – P highly significant, $P < 0.01$; P^{+3} – P very highly significant, $P > 0.001$; Student's t-test (Paired).

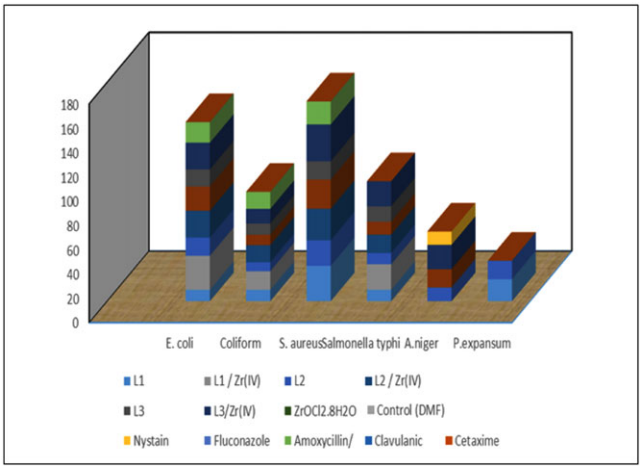

FIGURE 5 Statistical representation for biological activity of L_1, L_2, L_3 and their metal complexes

While the Zr(IV) – $(L_2)_2$ and Zr(IV) – $(L_3)_2$ chelates recorded the same result (22 mm) with the same strain and the free ligand achieved the lower result than their complexes. For *Coliform* ATCC8729 showed that highly significant for the complex of Zr(IV) – $(L_1)_2$ than its ligand. The complexes of other ligands Zr(IV) – $(L_2)_2$ and Zr(IV) – $(L_3)_2$ represented high results compared to other ligands respectively. Gram-positive bacteria *S. aureus* ATCC6538 recorded the best result with the complex of Zr(IV) – $(L_3)_2$ recording (30) followed by L_1 that recording (29) although its complex recording negative result for this strain while the complexes for Zr(IV), for L_2 obtained result higher its ligand. *Salmonella typhi* ATCC14028, that represent gram-negative bacteria, The complex of Zr (IV) – $(L_1)_2$ showed a significant difference that showed the highly results followed by complex Zr(IV) – $(L_3)_2$, then complex Zr(IV) – $(L_2)_2$,. So that the results ensured that, the three ligands recoding lower results than its complexes. The effect of different ligands and other complexes on the two testes fungal strains, *A. niger* recorded that Zr(IV) – $(L_3)_2$ showed a significant difference the highly results while the result of free its ligand showed result less than its complex. Others showed no any activity against tested fungi. The activity of different ligands and other complexes on *P. expansum* showed the highest broad spectrum of activity on L_1 followed by L_2.

Antimicrbial potency of standared antibiotics (AMC, CTX, NS, FU). The AMC mixture and NS recorded a less inhibitory activity than the synthesis ligands and its complexes on the tested microorganisms.

Finally, bacterial strains showed a varied response to the three free ligands and its complexes antimicrobial activity but the results ensured that the highly activity of the complexes better than its free ligands. The two fungal strains more resistance than bacterial strains on the synthesis ligands and its complexes.[39,40]

3.8 | Determination of MIC for the most sensitive organisms

The antimicrobial potency of the synthetic ligands and their complexes were determined against the most sensitive bacteria and fungi (Table (6A-6B-6C-6D) and Figure 6). The lowest MIC for *E. coli* against the ligands and their complexes recorded that L_3 and its complex at

concentration 0.02 mg/100 ml followed by L_2 at conc. 0.05 mg/100 ml then the complex Zr(IV) for L_1 at conc. 0.07 mg/100 ml. Finally, L_1 and the complex of Zr(IV) for L_2 recorded MIC at the conc. 0.1 mg/ 100 ml. The lowest MIC for *Coliform* against the ligands and their complexes recorded that L_2 and their complexes at concentration 0.02 mg/100 ml then followed by the complex of Zr(IV) for L_1 at conc. 0.05 mg/100 ml while the complex of Zr(IV) for L_3 at conc. 0.07 mg/100 ml recorded the best MIC. Finally, L_1 recorded MIC at the conc. 0.1 mg/100 ml. The MIC for *Salmonella typhi* showed that, the best results of ligands and their complexes L_3 and their complex also the complexe of Zr(IV) for L_2 at conc. 0.02 mg/100 ml. On the other hand, the ligands L_1 and L_2 recorded the MIC at conc. 0.07 mg/ 100 ml while the complex of Zr(IV) for L_1 showed the MIC at 0.1 mg/100 ml. The determination of MIC for *S. aureus* recorded the lowest conc. 0.02 mg/ 100 ml for the complex Zr(IV) for L_2 while the Ligand (L_3) and their complexes showed the MIC at conc. 0.07 mg/100 ml. Other ligands as L_1 and L_2 recorded MIC at 0.1 mg/100 ml while the complex of Zr(IV) for L_1 shows no activity for *S. aureus*.

TABLE 6A Of One-way ANOVA: E. coli versus MIC Compounds

Grouping Information Using the Fisher LSD Method			
Compounds	**N**	**Mean**	**Grouping**
L_3	3	0.02	A
Zr (IV)- L_3	3	0.02	A
L_2	3	0.05	B
Zr (IV)- L_1	3	0.07	B
L_1	3	0.10	C
Zr (IV)- L_2	3	0.10	C

Means that do not share a letter are significantly different

Fisher 95% Simultaneous Confidence Intervals

TABLE 6B Of One-way ANOVA: Coliform versus MIC Compounds

Grouping Information Using the Fisher LSD Method			
Compounds	**N**	**Mean**	**Grouping**
Zr (IV)- L_1	3	0.02	A
Zr (IV)- L_2	3	0.02	A
L_3	3	0.05	B
Zr (IV)- L_3	3	0.05	B
L_2	3	0.07	C
L_1	3	0.10	D

Means that do not share a letter are significantly different

Fisher 95% Simultaneous Confidence Intervals

Data in Table (6E-6F) and Figure 7 showed that the lowest MIC for the two tested strains at conc. 0.02 mg/100 ml at the L_2 then Zr(IV) for L_3 at conc. 0.02 mg/100 ml. The ligand L_1, its complex, L_3 and the complex of Zr(IV) for L_2 showed no activity against the tested strains. These results ensured that the activity of synthetic ligands and their complexes

TABLE 6C Of One-way ANOVA: S. aureus versus MIC Compounds

Grouping Information Using the Fisher LSD Method			
Compounds	**N**	**Mean**	**Grouping**
Zr (IV)- L_2	3	0.02	A
L_3	3	0.07	B
Zr (IV)- L_3	3	0.07	B
L_1	3	0.10	C
L_2	3	0.10	C
Zr (IV)- L_1	3	0.00	D

Means that do not share a letter are significantly different

Fisher 95% Simultaneous Confidence Intervals

TABLE 6D of One-way ANOVA: *Salm. typhi* versus MIC Compounds

Grouping Information Using the Fisher LSD Method			
Compounds	**N**	**Mean**	**Grouping**
L_1	3	0.02	A
Zr (IV)- L_2	3	0.02	A
L_3	3	0.02	A
Zr (IV)- L_3	3	0.02	A
L_2	3	0.07	B
Zr (IV)- L_1	3	0.10	C

Means that do not share a letter are significantly different

Fisher 95% Simultaneous Confidence Intervals

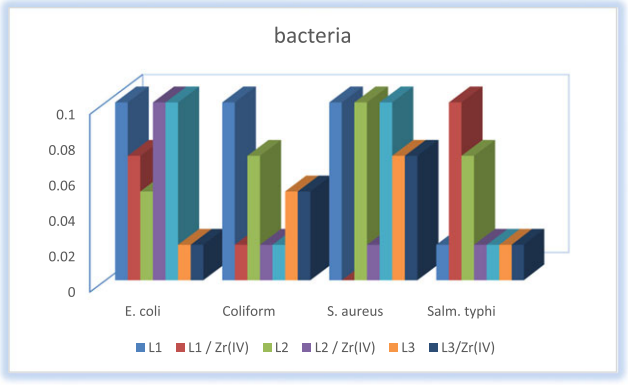

FIGURE 6 MIC for the most sensitive bacteria of L_1, L_2, L_3 and their complexes

on the pathogenic bacteria and fungi and showed the most sensitive pathogens dedicated the minimum inhibitory concentration (MIC).

TABLE 6E Of One-way ANOVA: *A.niger* versus MIC Compounds

Grouping Information Using the Fisher LSD Method			
Compounds	**N**	**Mean**	**Grouping**
L_2	3	8.00	B
Zr (IV)- L_3	3	10.00	C
L_3	3	0.00	D
Zr (IV)- L_2	3	0.00	D
Zr (IV)- L_1	3	0.00	D
L_1	3	0.00	D

Means that do not share a letter are significantly different

Fisher 95% Simultaneous Confidence Intervals

TABLE 6F Of One-way ANOVA: P.expansum versus MIC Compounds

Grouping Information Using the Fisher LSD Method			
Compounds	**N**	**Mean**	**Grouping**
L_1	3	8.0	A
L_2	3	7.0	A
Zr (IV)- L_1	3	0.0	B
Zr (IV)- L_2	3	0.0	B
L_3	3	0.0	B
Zr (IV)- L_3	3	0.0	B

Means that do not share a letter are significantly different

Fisher 95% Simultaneous Confidence Intervals

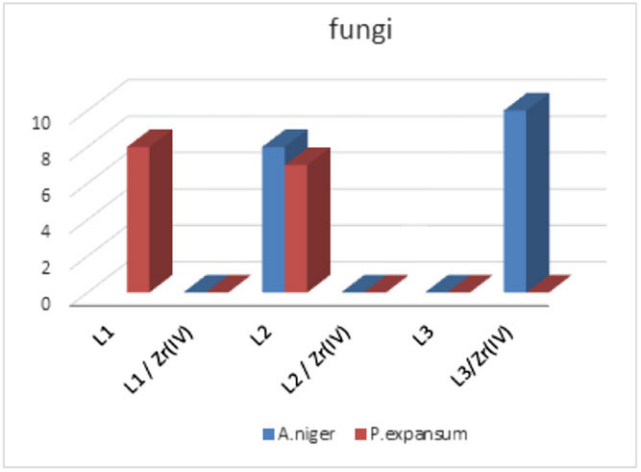

FIGURE 7 MIC for the most sensitive fungi of L_1, L_2, L_3 and their complexes

3.9 | Cytotoxic activity

The *in vitro* growth inhibitory activity of the prepared compounds was tested using crystal violet colorimetric viability assay (Doxorubicin standard drugs). Generated data were carried to plot a dose–response curve, which the concentration of prepared compounds required to kill 50% of cell population (IC_{50}) had measured and the results showed that all the tested compounds have inhibitory activity in a tumor cell lines in a concentration dependent manner. Cytotoxic activity was referring to the mean IC_{50} of three independent experiments. The results are shown in Table 7 and Figure 8 showing that

TABLE 7 The *in vitro* inhibitory activity of free three ligands and their metal complexes against tumor cell line expressed as IC_{50} values (μg/ml) ± standard deviation from six replicates

	Tumor cell lines	
Tested compounds	**HCT-116**	**S.D. (±)**
L_1	148.0	0.6
$[ZrO(L_1)_2Cl]Cl{\cdot}H_2O$	53.2	0.7
L_2	110.0	1.1
$[ZrO(L_2)_2Cl]Cl{\cdot}H_2O$	46.9	0.2
L_3	60.8	0.2
$[ZrO(L_3)_2Cl]Cl{\cdot}H_2O$	28.3	0.4
Doxorubicin standard	0.46	0.1
5-Flurouracil standard	3.9	0.1

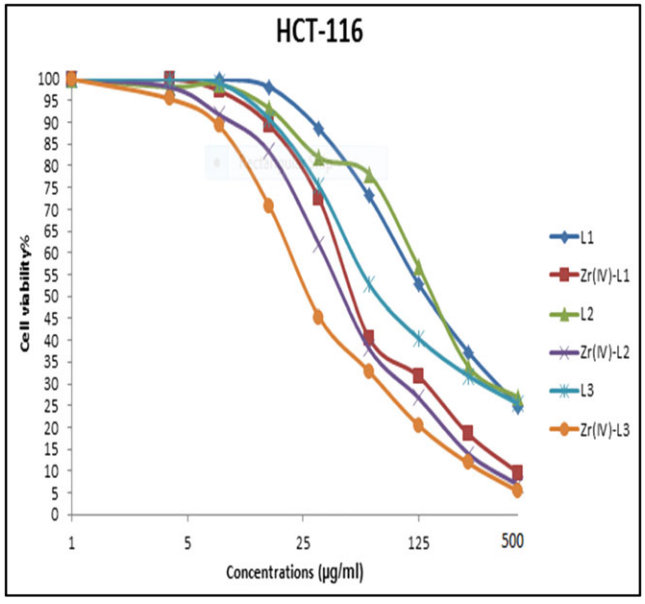

FIGURE 8 The dose response curve showing the *in vitro* inhibitory activity of free three ligands and its metal complexes against human colon carcinoma (HCT-116) cell line

free three ligand (L_1, L_2 and L_3), the parent compound showed inhibitory activities with IC_{50} values of 148.0, 110.0 and 60.8 μg/ml against colon cell line, respectively. The tested compounds showed high inhibitory activities against a human colon carcinoma (HCT-116) cell line. $[ZrO(L_3)_2Cl]Cl{\bullet}H_2O$ was the most active against HCT-116 followed by $[ZrO(L_2)_2Cl]Cl{\bullet}H_2O$ and $[ZrO(L_1)_2Cl]Cl{\bullet}H_2O$ with IC_{50} values 28.3, 46.9 and 53.2 μg/ml, respectively.

4 | CONCLUSION

The preparation and characterization of three novel complexes of some substituted pyrazole derivatives as ligands (4-[2-vinylthiophene]-3-methyl pyrozolin-5(4H) - one (L_1), 4-[4-chloro benzylidine]-3-methyl pyrozolin-5(4H) - one (L_2) and 4-[4-dimethylnitro benzylidine]-3-methylpyrozolin-5(4H)- one (L_3)) with Zr (IV) metal ion have been achieved with physicochemical and spectroscopic methods. In the resultant complexes, L_1, L_2, and L_3 were bound to metal ion via the two nitrogen atoms of ν(C=N) and ν (N-H). The kinetic parameters of thermogravimetric and its differential were evaluated using Coats-Redfern and Horowitz-Metzger equations for three ligands and their complexes. The metal complexes exhibits higher inhibition against all microorganisms tested and on the pathogenic bacteria and fungi and showed the most sensitive pathogens dedicated the minimum inhibitory concentration (MIC) as well as $[ZrO(L_3)_2Cl]Cl{\bullet}H_2O$ complex exhibited a higher antitumor activity than other complexes compared to free L_1, L_2, and L_3 ligands.

ACKNOWLEDGEMENTS

The authors gratefully acknowledge the Central Laboratory of Medicine Ministry for performing the antimicrobial measurements. The authors are thankful to Zagazig University, Egypt for the support of this research work.

CONFLICT OF INTEREST

This research holds no conflict of interest and is not funded through any source.

ORCID

Walaa H. El-Shwiniy http://orcid.org/0000-0002-7577-8090

REFERENCES

[1] H. Chen, Z. Li, Y. Han, *J. Agric. Food Chem.* **2000**, *48*, 5312.

[2] G. Meaza, F. Bettarini, L. P. Porta, P. Piccardi, E. Signorini, D. Portoso, L. Fornara, *Pest Manag. Sci.* **2004**, *60*, 1178.

[3] H. Dai, S. S. Ge, J. Guo, S. Chen, M. L. Huang, J. Y. Yang, S. Y. Sun, Y. Ling, *Eur. J. Med. Chem.* **2018**, 143,1066.

[4] M. G. Prabhudeva, S. Bharath, A. D. Kumar, S. Naveen, N. K. Lokanath, B. N. Mylarappa, K. A. Kumar, *Bioorg. Chem.* **2017**, *73*, 109.

[5] H. Dai, S. S. Ge, G. Li, J. Chen, Y. J. Shi, L. Y. Ye, Y. Ling, *Bioorg. Med. Chem. Lett.* **2016**, *26*, 4504.

[6] H. Dai, W. Yao, Y. Fang, S. Y. Sun, Y. J. Shi, J. Chen, G. Q. Jiang, J. Shi, *Molecules* **2017**, *22*, 2000.

[7] H. Dai, G. Li, J. Chen, Y. J. Shi, S. S. Ge, C. G. Fan, H. B. He, *Bioorg. Med. Chem. Lett.* **2016**, *26*, 3818.

[8] H. Dai, J. Chen, H. Li, B. J. Dai, Y. Fang, Y. J. Shi, *Molecules* **2016**, *22*, 276.

[9] H. Dai, J. Chen, G. Li, S. S. Ge, Y. J. Shi, Y. Fang, Y. Ling, *Bioorg. Med. Chem. Lett.* **2017**, *27*, 950.

[10] G. P. Ouyang, Z. Chen, X. J. Cai, B. A. Song, P. S. Bhadury, S. Yang, L. H. Jin, W. Xue, D. Y. Hu, S. Zeng, *Bioorg. Med. Chem.* **2008**, *16*, 9699.

[11] L. Clemens, *Heterocycles* **2007**, *71*, 1467.

[12] J. A. Marsella, K. G. Moloy, K. G. Kaulton, *J. Org. Chem.* **1980**, 201,389.

[13] L. Knorr, *Ber. Dtsch. Chem. Ges.* **1883**, *16*, 2597.

[14] E. Knovenagel, *Ber. Dtsch. Chem. Ges.* **1898**, *31*, 2596.

[15] B. S. Furniss, A. J. Hannaford, P. W. G. Smith, A. R. Patchel, *Vogel's Textbook of Practical Organic Chemistry*, 5th ed. Vol. 136, Longman Singapore Publishers Pvt. Ltd. **1996**, 23.

[16] J. March, *Advanced Organic Chemistry: Reactions, Mechanisms and Structures*, 4th ed., John Wiley & Sons, Inc., New York **1992**, 937.

[17] G. Mariappan, B. P. Saha, L. Sutharson, A. Singh, S. Garg, L. Pandey, D. Kumar, *Saudi Pharm. J.* **2011**, *19*, 115.

[18] G. Mariappan, B. P. Saha, L. Sutharson, A. S. Garg, L. D. Kumar, A. Review, *J. Pharm. Res.* **2010**, *3*, 2856.

[19] O. A. Georgewill, U. O. Georgewill, R. N. P. Nwankwoala, *Int. J. Pharmacol.* **2009**, *7*, 6.

[20] H. G. Aslan, Z. Onal, *Med. Chem. Res.* **2014**, *23*, 2596.

[21] S. A. Sadeek, S. M. Abd El-Hamid, W. H. El-Shwiniy, *Res. Chem. Interm.* **2016**, *42*, 3183.

[22] Y. Saintigny, R. J. Monnat Jr., *Sci. Aging Knowledge Environ.* **2004**, *13*, 1.

[23] W. J. Geary, *Coord. Chem. Rev.* **1971**, *7*, 81.

[24] K. Bürger, *Coordination Chemistry: Experimental Methods*, Butterworth, London **1973**.

[25] M. S. Refat, *J. Mol. Struct.* **2007**, *24*, 842.

[26] M. S. Refat, *Spectrochim. Acta A* **2007**, *68*, 1393.

[27] E. M. Nour, I. S. Alnami, N. A. Alem, *J. Phys. Chem. Solid* **1992**, *53*, 197.

[28] S. A. Sadeek, W. H. El-Shwiniy, *J. Coord. Chem.* **2010**, *63*, 347.

[29] A. Syamal, P. O. Singhal, S. Banerjee, *Synth. React. Inorg. Met.-Org. Chem.* **1980**, *243*, 10.

[30] M. Y. Nassar, W. H. El-Shwiniy, A. M. El-Sharkawy, S. I. El-Desoky, *J. Iran. Chem. Soc.* **2018**, *15*, 269.

[31] S. P. McGlynnm, J. K. Smith, W. C. Neely, *J. Chem. Phys.* **1961**, *35*, 105.

[32] L. H. Jones, *Spectrochim. Acta A* **1958**, *10*, 395.

[33] L. H. Jones, *Spectrochim. Acta A* **1959**, *11*, 409.

[34] K. Nakamoto, *Infrared and Raman Spectra of Inorganic and Coordination Compounds*, 4th ed. Vol. 230, Wiley, New York **1986**.

[35] N. Sultana, M. S. Arayne, S. Gul, S. Shamim, *J. Mol. Struct.* **2010**, *975*, 285.

[36] W. A. Zordok, W. H. El-Shwiniy, M. S. El-Attar, S. A. Sadeek, *J. Mol. Struct.* **2013**, 267, 1047.

[37] A. W. Coats, J. P. Redfern, *Nature* **1964**, *68*, 201.

[38] H. W. Horowitz, G. Metzger, *Anal. Chem.* **1963**, *35*, 1464.

[39] E. K. Efthimiadou, N. Katsaros, A. Karaliota, G. Psomas, *Bioorg. Med. Chem. Lett.* **2007**, *17*, 1238.

[40] N. Dharmaraj, P. Viswanathamurthi, K. Natarajan, *Transition Met. Chem.* **2001**, *26*, 105.

SUPPORTING INFORMATION

Additional supporting information may be found online in the Supporting Information section at the end of the article.

How to cite this article: El-Shwiniy WH, Shehab WS, Mohamed SF, Ibrahium HG. Synthesis and cytotoxic evaluation of some substituted pyrazole zirconium (IV) complexes and their biological assay. *Appl Organometal Chem*. 2018;e4503. https://doi.org/10.1002/aoc.4503